Root-associated *Streptomyces* produce galbonolides to modulate plant immunity and promote rhizosphere colonisation

Clément Nicolle[1], Damien Gayrard[1,2], Alba Noël[3], Marion Hortala[1], Aurélien Amiel[1,2], Sabine Grat[1], Aurélie Le Ru[4], Guillaume Marti[1,5,6], Jean-Luc Pernodet[3], Sylvie Lautru[3], Bernard Dumas[1*], Thomas Rey[1,2*]

AFFILIATIONS

1 Laboratoire de Recherche en Sciences Végétales, Université de Toulouse, CNRS, Université Toulouse III, Toulouse INP, 24 Chemin de Borde Rouge, Auzeville, 31320, Auzeville-Tolosane, France

2 DE SANGOSSE, Bonnel, 47480, Pont-Du-Casse, France

3 Université Paris-Saclay, CEA, CNRS, Institute for Integrative Biology of the Cell (I2BC), 91198, Gif-sur-Yvette, France

4 Plateforme d'Imagerie FRAIB-TRI, Université de Toulouse, CNRS, Auzeville-Tolosane 31320, France

5 Metatoul-AgromiX Platform, LRSV, Université de Toulouse, CNRS, UPS, Toulouse INP, Toulouse, France,

6 MetaboHUB-MetaToul, National Infrastructure of Metabolomics and Fluxomics, Toulouse, France

***Contributed equally**

CORRESPONDING AUTHOR'S EMAIL

bernard.dumas@univ-tlse3.fr

reyt@desangosse.com

LEAD CONTACT

Further information and requests for resources and reagents should be directed to the lead contact Thomas Rey. reyt@desangosse.com

SHORT TITLE

Galbonolides from rhizosphere *Streptomyces*

KEY WORDS

Rhizosphere, Galbonolides, *Streptomyces*, *Arabidopsis*, Camalexin

ABSTRACT

The rhizosphere, which serves as the primary interface between plant roots and the soil, constitutes an ecological niche for a huge diversity of microbial communities. Currently, there is little knowledge on the nature and the function of the different metabolites released by rhizospheric microbes to facilitate colonization of this highly competitive environment. Here, we demonstrate how the production of galbonolides, a group of polyene macrolides that inhibit plant and fungal Inositol Phosphorylceramide Synthase (IPCS), empowers the rhizospheric *Streptomyces* strain AgN23, to thrive in the rhizosphere by triggering the plant's defence mechanisms. Metabolomic analysis of AgN23-inoculated *Arabidopsis* roots revealed a strong induction in the production of an indole alkaloid, camalexin, which is a major phytoalexin in *Arabidopsis*. By using a plant mutant compromised in camalexin synthesis, we show that camalexin production is necessary for the successful colonization of the rhizosphere by AgN23. Conversely, hindering galbonolides biosynthesis in AgN23 knock-out mutant resulted in loss of inhibition of IPCS, a deficiency in plant defence activation, notably the production of camalexin, and a strongly reduced development of the mutant bacteria in the rhizosphere. Together, our results identified galbonolides as important metabolites mediating rhizosphere colonisation by *Streptomyces*.

INTRODUCTION

Cross-kingdom communications play a significant role in shaping interactions between organisms within diverse ecological niches (Mendes and Raaijmakers 2015). Microbe-microbe communication is often mediated by the secretion of small and diffusible specialised metabolites (Andrić et al 2021, Andrić et al 2023, Getzke et al 2023, Krespach et al 2021, Krespach et al 2023) . Throughout their lifecycle, eukaryotic organisms such as plants, are known to associate with the abundant and diverse community of microorganisms (Chaparro et al 2014, Durán et al 2018, Fitzpatrick et al 2018). However, there is currently limited knowledge on how plants establish communication with microorganisms and regulate their populations in and around their tissues (Fitzpatrick et al 2020). It has been noted that

56 plants, even when grown in geographically distant soils, tend to assemble a core microbiota
57 comprising bacteria, fungi and oomycetes, suggesting the existence of broad trans-kingdom
58 communication mechanisms within plant-microbe interactions (Thiergart et al 2020). In this context,
59 it becomes primordial to understand the molecular basis of plant-microbiota assembly to achieve the
60 intelligent engineering of crops microbiota (Russ et al 2023). Such approach would be an important
61 milestone towards sustainable agricultural practices in nutrition and protection against pathogens and
62 abiotic stresses (Berendsen et al 2018, Busby et al 2017). An example of this approach is the recently
63 reported study on how a *Streptomyces* strain alleviates abiotic stress in a plant by producing pteridic
64 acid (Yang et al 2023).

65 The *Streptomyces* genus belongs to Actinomycetes, a family of filamentous sporulating Gram+
66 bacteria which constitutes the second most prominent component of root microbiota after
67 proteobacteria (Bulgarelli et al 2012, Lebeis et al 2015, Ling et al 2022). Among Actinomycetes,
68 *Streptomyces* spp. are enriched in endophytic and epiphytic root compartments and represent up to
69 30% of the total bacterial Operational Taxonomic Units (OTUs)(Lundberg et al 2012). Enrichment of
70 *Streptomyces* spp. in soil and rhizosphere correlates with resistance to drought and pathogen attack
71 (Cha et al 2016, Fitzpatrick et al 2018). Furthermore, streptomycetes are hallmark producers of
72 antimicrobial specialised metabolites involved in protection against plant pathogens (Avalos et al
73 2020, Cordovez et al 2015, Kim et al 2019). *Streptomyces* spp. have also been demonstrated to elicit
74 Salicylic Acid (SA) and ISR (Induced Systemic Resistance) dependent responses leading to the
75 activation of plant defence metabolism (Conn et al 2008, Kurth et al 2014). These important attributes
76 have stimulated great interest in the use of streptomycetes for crop protection (Rey and Dumas 2017,
77 Viaene et al 2016).

78 In a previous paper, we reported the screening of a collection of 35 *Streptomyces* strains isolated from
79 agricultural soils for their plant defence elicitation (Vergnes et al 2020). Among these, the AgN23 strain
80 has been reported to display a remarkable potential to elicit *Arabidopsis* defences associated to

81 salicylate, jasmonate and ethylene signalling (Vergnes et al 2020). Foliar inoculation with the bacteria
82 resulted in the formation of *SALICYLIC INDUCTION DEFICIENT 2 (SID2)* dependent necrotic symptoms
83 in *Arabidopsis* and protection against *Alternaria brassicicola* colonisation (Vergnes et al 2020). A
84 recent analysis of the AgN23 genome showed that the strain belongs to the clade *S. violaceusniger*
85 (Gayrard et al 2023). The AgN23 genome harbours large gene families associated to rhizosphere
86 colonization, such as biosynthetic gene clusters (BGCs) involved in the synthesis of plant bioactive and
87 antimicrobial compounds, plant cell wall degrading enzymes, and phytohormone synthesis.

88 In this work, we investigate the molecular basis of AgN23 interaction with plant roots by characterising
89 rhizosphere colonisation by the bacteria and the resulting plant responses. We find that AgN23
90 triggered plant biosynthesis of the antimicrobial camalexin and show that this phytoalexin is an
91 important feature for rhizosphere colonisation by the *Streptomyces*. In addition, we established that
92 AgN23 produce galbonolides that can interfere with plant sphingolipid metabolism by targeting the
93 Inositol Phosphorylceramide Synthase. Finally, we show that galbonolides biosynthesis by AgN23 is
94 instrumental for plant defence stimulation, including camalexin production and rhizosphere
95 colonisation by the bacterium.

96 **MATERIAL AND METHODS**

97 **Plant material, growth conditions and phenotyping**

98 Seeds of *Arabidopsis thaliana* accession Col-0 (N1092) were obtained from the Nottingham
99 Arabidopsis stock center (NASC) and mutant *pad3-1* (N3805) were kindly provided by Dr. Pawel
100 Bednarek. *Arabidopsis* plants grown in potting soil (PROVEEN; Bas Van Buuren B.V., Holland) were
101 cultivated in a growth chamber under 16 hours photoperiod and 23 °C unless otherwise indicated.
102 Similar conditions were applied to the cultivation of *Nicotiana benthamiana*. One-month-old *N.*
103 *benthamiana* leaves were syringe-infiltered with bacterial CMEs. Cell death areas were photographed
104 24–48 hours after infiltration, with an Expression 11000 XL scanner (Epson) at 300 dots/inch.

105 To perform soil inoculation assays with AgN23, 70 g of potting soil inoculated with AgN23 spore
106 inoculum at 10^4 CFU/g was distributed in pots placed in small plastic bags to avoid cross-contamination
107 during watering. 5 to 10 *Arabidopsis* seeds were sown per pot and the pots were placed in a growth
108 phytotronic chamber. A single seedling was kept per pot 5 days after germination. Pots were watered
109 weekly with 10 mL of tap water. The watering pots were photographed to monitor the aerial part
110 phenotype. Green area was measured with ImageJ (v. 1.51k) at 4, 6 or 7 weeks after inoculation.
111 Details regarding *in vitro* cultivation of *Arabidopsis* are in Supplementary methods.

112 **AgN23 cultivation and transgenesis to obtain reporter lines and Δ*gbnB* mutants**

113 AgN23 was grown in Bennett medium for the purpose of liquid state cultivation and of Culture Media
114 Extract (CME) production (D-Glucose 10 g/L; Soybean peptones 2.5 g/L; Yeast Extract 1.5 g/L; Sigma).
115 The culture was set in 250 mL Erlenmeyer flasks by inoculating 50 mL Bennett medium with 100 µL of
116 fresh spore suspension at 10^5 CFU/mL at 250 rpm and 28 °C in a shaking incubator at 250 rpm for 7
117 days. For the purpose of spore production and genetic manipulations AgN23 strain was cultivated on
118 the solid medium Soya Flour Mannitol (SFM) medium (D-Mannitol (Sigma) 20 g/L; organic soya flour
119 (Priméal) 20 g/L; BactoTM Agar (Difco Laboratories) 20 g/L).

120 *Escherichia coli* strains were grown in LB with appropriate antibiotics as necessary. *E. coli*
121 transformation and *E. coli* / *Streptomyces* conjugation were performed according to standard
122 procedures (Kieser et al 2000, Sambrook et al 2000). Phusion High-fidelity DNA Polymerase (Thermo
123 Fisher Scientific) was used to amplify DNA fragment except for PCR verification of plasmids or strains
124 for which Taq polymerase (Qiagen) was used. DNA fragments and PCR products were purified using
125 the Nucleospin Gel and PCR clean up kit (Macherey-Nagel).

126 For pOSV700 plasmid construction, a 0.4 kb DNA fragment encompassing the ermEp* promoter and
127 the tipA ribosome binding site (RBS) was amplified from pOSV666 using the primers JWseq6 and
128 JWseq7. The fragment was digested by EcoRV and cloned into EcoRV-digested pSET152, resulting in
129 pOSV700. The sequence of the insert was verified.

130 For GFP and mCherry transgenesis, the sequences of the soluble-modified GFP (smGFP) and mCHERRY
131 genes were optimized for expression in *Streptomyces*, synthesized as gblocks (IDT) and cloned into
132 pGEM-T easy, resulting in pmsolGFP and pmCHERRY, respectively. The smGFP and mCHERRY genes
133 were amplified from these plasmids using the primer pairs onSC001/onSC011 and onSC005/onSC013,
134 respectively. PCR amplicons were digested by NdeI and PacI and cloned into NdeI/PacI-digested
135 pOSV700. The resulting plasmids were verified by restriction digestion and sequencing, and named
136 pSC001 (smGFP) and pSC003 (mCHERRY). These were subsequently introduced in *E. coli*
137 ET12567/pUZ8002 and transferred into *Streptomyces* sp. AgN23 by intergeneric conjugation.
138 Conjugants were selected on apramycin 50 µg/ml. The resulting strains were verified by PCR on the
139 extracted genomic DNA using the pSET152-F and pSET152-R primers.

140 For production of galbonolides knock-out mutants, a 5 kb internal fragment of *gbnB* coding for the
141 structural PKS gene of the galbonolides biosynthetic gene cluster was replaced by a kanamycin
142 resistance cassette. For this purpose, a 2kb fragment (upstream fragment) encompassing the
143 beginning of *gbnB* was amplified by PCR with the onSC007/onSC008 primer pair and cloned into
144 pGEM-T Easy, yielding pSC008. Similarly, a 2kb fragment (downstream fragment) encompassing the
145 end of *gbnB* was amplified by PCR with the onSC009/onSC010 primer pair and cloned into pGEM-T
146 Easy, yielding pSC009. The pSC008 and pSC009 plasmids were digested by EcoRI/EcoRV and
147 DraI/HindIII, respectively, and the 2 kb fragments (upstream and downstream fragments respectively)
148 were purified on agarose gel. The kanamycin resistance cassette was obtained by digesting pOSV514
149 by EcoRV. The three fragments (upstream, downstream and resistance cassette) were next ligated
150 into EcoRI/HindIII-digested pOJ260. The resulting plasmid, named pSC004, was verified by digestion
151 with BamHI, PstI, EcoRI and EcoRV. Five independent conjugants were verified by PCR using the
152 onSC022/onSC023, onSC021/JWseq16, and onSC030/JWseq17 primer pairs. All oligonucleotides used
153 in this work are listed in Supplementary Table S5.

154

155 **Analysis of *Arabidopsis* defence response**

156 Detailed procedures for *Arabidopsis* loss of electrolytes and Calcium signal detection are described in
157 Supplementary Methods. For defence gene expression assays, total RNAs were extracted using the
158 RNeasy Plant Mini Kit (Qiagen) and DNase treated with RQ1 RNase-Free DNase (Promega). For each
159 sample, 1 µg of total RNA was reverse-transcribed with the High Capacity cDNA Reverse Transcription
160 Kit (Applied Biosystems). cDNAs were diluted to 1 ng/ µL and used for qPCR analysis in a 10 µL reaction
161 mix containing 5 µL of LightCycler® 480 SYBR Green I Master mix (Roche), 300 nM of each primer, and
162 2 µL of the diluted template cDNAs. qPCR was performed in triplicate using a LightCycler ® 480 System
163 (Roche) with preheating at 95 °C for 5 minutes and then 40 cycles of 95 °C for 15 s and 60 °C for 60 s.
164 The Polyubiquitin 10 gene AT4G05320 was retained for normalization. The 2-ΔCp method was used
165 to display gene expression levels 82. Primers used in this study are listed in Supplementary Table S5.

166 **AgN23 DNA quantification from soil and rhizosphere DNA**

167 To track the development of AgN23, the plants were removed from the soil. The remaining soil from
168 each pot was homogenized and a small amount was sampled and considered as bulk sample. Roots
169 were placed into 50 mL conical sterile polypropylene centrifuge tubes filled with 20 mL 1X phosphate-
170 buffered saline (pH 7.4), and vigorously vortexed to release the adhering rhizospheric soil. Tubes were
171 then centrifuged at 4000 rpm and the washing step was repeated one time. Soil pellets after second
172 centrifugation step were considered as rhizosphere samples. Samples were stored at -80°C until
173 processing. The total microbe DNA from 100 mg of bulk or rhizosphere samples was extracted using
174 the *Quick*-DNATM Fecal/Soil Microbe Miniprep kit (Zymo Research) following manufacturer's
175 instructions. DNA was eluted in 100 µL DNA Elution Buffer and quantified with DS-11
176 Spectrophotometer/Fluorometer (DeNovix) and stored at -80°C until processing. The experimental
177 procedures and calculation for AgN23 genome copies quantification in the rhizosphere is detailed in
178 Supplementary methods.

179

180 **Preparation of samples for biochemistry studies and mass spectrometry analysis**

181 For root metabolome studies, 10 *Arabidopsis* seedlings from the same MS plate were sampled
182 together in 2 mL microtubes containing two 3 mm-diameter tungsten carbide beads (Qiagen), and
183 flash frozen in liquid nitrogen. For studies of AgN23 culture media extract (CME), the bacterial biomass
184 grown in liquid flask culture was removed from the culture supernatant by centrifugation at 4,200 rpm
185 for 10 min, completely dried in oven at 50 °C, and weighed to assess AgN23 growth. Further details
186 regarding metabolites extraction of AgN23 and *Arabidopsis* are detailed in Supplementary methods.

187 **Microscopy**

188 For stereo microscopy, we used a Nikon SMZ16 microscope equipped with a camera. Confocal
189 microscopy was performed on a TCS SP8 confocal microscope (Leica, Microsystems, UK). For GFP-
190 tagged AgN23 cells, the excitation wavelength was 488 nm, with emission absorbance between 500
191 nm and 550 nm, whereas an excitation wavelength of 543 nm was used for mCherry-tagged AgN23
192 cells proteins, with emission absorbance between 560 nm and 600 nm. Images were acquired with a
193 ×40 or ×20 water immersion lens. All confocal images were analysed and processed using the ImageJ
194 software package (http://rsb.info.nih.gov/ij/; v. 1.51k).

195 ***Arabidopsis* Inositol Phosphorylceramide Synthase inhibition assay**

196 To study the effect of AgN23 CME on *Arabidopsis* IPCs, we purified microsomal fractions of transgenic
197 yeast expressing AtIPCS2 (AT2G37940) in enzymatic activity assays. First, a preculture of yeast MSY23-
198 3C pESC-LEU_AtIPCS2 strain was performed by picking a single colony and propagating it in 5 mL SGR
199 -TRP -LEU medium (0.1% galactose, 1% raffinose)(Pinneh et al 2019). The preculture was incubated at
200 30 °C, 200 rpm until the OD_{600} reached 0.8. The preculture was then mixed with 245 mL of fresh SGR
201 medium and incubated at 30 °C, 200 rpm until the OD_{600} reached 0.8. Yeast cells were then harvested
202 by centrifugation, washed with cold phosphate-buffered saline, and stored at -80 °C until microsome
203 preparation. Crude microsomal membranes from yeast MSY23-3C pESC-LEU_AtIPCS2 strain were
204 prepared as previously described with additional CHAPSO washing steps (Mina et al 2010). Total

205 protein quantification was performed by Bradford assay and aliquots at 0.5 mg/mL were made and
206 stocked at -80 °C. Details regarding analytical parameters to study AtIPCS2 enzymatic activity are
207 described in Supplementary methods.

208 **RESULTS**

209 **AgN23 colonises *Arabidopsis* rhizodermis and rhizosphere**

210 In view of the fact that AgN23 was isolated from grapevine rhizosphere, we looked into the interaction
211 of the strain with roots by inoculating *in vitro* grown *Arabidopsis thaliana* Col-0 seedlings with AgN23
212 spores. A drop of the spore suspension was deposited at the root tip of young seedlings. A strong
213 development of bacterial microcolonies was observed at the inoculation site 10 days after inoculation
214 (Figure 1a). We generated GFP and RFP-labelled transgenic AgN23 strains and observed the
215 colonization patterns of both strains by epifluorescence microscopy. Results showed that bacteria can
216 spread beyond the initial inoculation spot and colonise other developing sections of the root system,
217 such as lateral roots and apical meristem (Figure 1b). Visual and microscopic inspection of the AgN23-
218 treated plants suggested that the inoculated bacteria did not lead to any characteristic symptoms such
219 as root browning or rhizodermis damages in *Arabidopsis*. Moreover, penetration of AgN23 into the
220 root tissues was not observed. Nevertheless, we observed that AgN23 inoculation did result in a slight
221 (about 10%) reduction in root elongation (Figure 1c).

222 To study the colonization of the rhizosphere by AgN23, we inoculated potting soil with 10^5 AgN23
223 spores/g of soil prior to sowing Arabidopsis seeds. Consistent with our previous *in vitro* observation,
224 the presence of AgN23 reduced rosette growth without causing obvious symptoms to the leaves
225 (Figure 1d, 1e) (Vergnes et al, 2020). The development of AgN23 in the inoculated soil was monitored
226 by extracting microbial DNA from both unplanted and rhizosphere soil samples. A quantification of
227 AgN23 genome copies was implemented by amplifying a specific genomic region of the strain from
228 soil samples and from a standard curve of AgN23 purified DNA. Knowing the molecular weight of
229 AgN23 genome, we extrapolated genome copies number from the estimated mass of AgN23 DNA

230 detected in soil. A total of $3.06x10^8$ genome copies of AgN23 were detected in the unplanted soil 7
231 weeks post inoculation, whereas $1.87x10^{10}$ genome copies of the bacteria were detected in the
232 rhizosphere. This shows that AgN23 preferentially colonised the *Arabidopsis* rhizosphere rather than
233 the unplanted soil (Figure 1F). Taken together, our data confirm that AgN23 is an epiphytic and
234 rhizospheric bacterium that triggers slight reduction in plant growth, albeit without symptoms.

235 **Activation of camalexin biosynthesis by AgN23 promotes bacteria settlement in the rhizosphere**

236 In a previous work, we characterised the plant defence stimulating activity of AgN23 and found that
237 the bacterial culture media extract (CME) induced robust transcriptional responses associated with
238 *Arabidopsis* specialized metabolism (Vergnes et al 2020). Detailed analysis showed transcriptional
239 induction of genes coding enzymes involved in camalexin biosynthesis following treatment with
240 AgN23 CME after 1 and 6 hours post-treatment which is a major phytoalexin of *Arabidopsis* belonging
241 to indole alkaloid (Supplementary Figure S1).

242 To analyse the metabolomic response of root tissues to AgN23, we extracted the metabolites from
243 whole seedlings cultivated *in vitro* in contact with AgN23 for 10 days. The extracts were subjected to
244 a full-scan LC-HRMS metabolomics analysis in ESI+ and ESI- modes and then combined in a single list
245 of variables. A total of 511 variables were retrieved across all the samples out of which, 416 received
246 level 3 annotations according the Metabolomic Standard Initiative based on internally built database
247 and the exact mass and fragmentation profile of the ions (Supplementary Table S1). Unsupervised PCA
248 of the complete variable dataset allowed us to clearly discriminate the control samples from those
249 inoculated with AgN23, with component 1 and component 2 supporting 32.9 % and 21.6% of the
250 variability, respectively (Supplementary Figure S2).

251 To identify the underlying chemical classes supporting the separation of control and AgN23 inoculated
252 samples, we computed the fold change for each individual variable between the two conditions.
253 Results showed that 20 and 39 metabolites were enriched in control and AgN23 conditions,
254 respectively (Supplementary Table S1). These metabolites were sorted based on their chemical

255 classes, revealing a strong induction of metabolites belonging to specialised metabolism, such as
256 indoles, flavonoids or fatty acyls (Figure 2a). A PLS-DA model was then built to identify the most
257 significant metabolites supporting samples separation (Figure 2b). It turned out that primary
258 metabolism markers (sucrose and glutamate) were enriched in the control root, suggesting that these
259 are depleted from the roots in presence of the bacteria. In contrast, camalexin and indol-3-yl-
260 methylglucosinolate (I3M) were the two most significant enriched metabolites in AgN23 treated roots.
261 This suggests that the biosynthesis of these two metabolites is induced by the bacteria. This conclusion
262 was further substantiated by comparing the peak areas corresponding to the two metabolites in mock
263 and AgN23 treated plants. In the presence of AgN23, 259.4 and 2.2-fold induction were noted for
264 camalexin and I3M, respectively (Figure 2c).

265 In view of the strong and specific production of camalexin in response to AgN23, we characterised the
266 behaviour of the *phytoalexin deficient mutant 3 (pad3-1),* mutated in a CYP450 coding gene which
267 converts cysteine-indole-3-acetonitrile to camalexin, in response to the bacteria (Schuhegger et al
268 2006). Metabolomics characterisation of *pad3-1* roots indicated that the metabolome of *pad3-1* upon
269 AgN23 inoculation was indistinguishable from that under mock conditions (Figure 2d, Supplementary
270 Table S2). We further validated the complete lack of induction of camalexin biosynthesis in *pad3-1*
271 (figure 2e).

272 Interestingly, we observed that *pad3-1* plants inoculated with AgN23 showed a phenotype similar to
273 that of the wild type Col-0 (Figure 3a, 3b) with respect to roots and rosette growth inhibitions (Figure
274 3c, 3d). To check if camalexin production had any effect on AgN23 multiplication in the rhizosphere,
275 we quantified AgN23 in the rhizosphere of the WT and the *pad3-1* mutant. Results showed that the
276 number of genome copies of AgN23 in the rhizosphere of *pad3-1* plant was 2.96 times lower than in
277 Col-0 (Figure 3e). Taken together with the data from *in vitro* inoculation, these results demonstrate
278 that the induction of camalexin synthesis promotes AgN23 colonisation in the rhizosphere.

279 **AgN23 produces galbonolides, polyketides capable of inhibiting plant Inositol Phosphorylceramide**
280 **synthase**

281 To identify AgN23 specialised metabolites that could be involved in elicitation of root metabolome
282 responses, we performed a LC-HRMS global metabolomics analysis. Briefly, apolar compounds of the
283 CME were adsorbed on XAD16 resin beads and extracted with butanol prior to preparation for full-
284 scan liquid chromatography high-resolution mass spectrometry (LC-HRMS). The samples were
285 injected in ESI+ and ESI- mode and combined in a single list of variables. A total of 1022 variables were
286 retrieved across all the samples and 812 received level 3 annotations according the Metabolomic
287 Standard Initiative based on internally built database and the exact mass and fragmentation profile of
288 the ions (Supplementary Table S3). This approach led to the putative identification of several
289 specialised metabolites that have been known to be produced by *Streptomyces* ssp. (Supplementary
290 Figure S3, Table 1).

291 Among these specialised metabolites, we identified the antifungal compounds niphimycin, nigericin
292 and galbonolides (also known as rustmicin). The identification of these specialised candidate
293 metabolites is consistent with the biosynthetic gene clusters (BGCs) that we recently annotated
294 (Gayrard et al 2023). Among the three compounds, galbonolides were originally reported for their
295 inhibitory activities against fungal and in plants Inositol Phosphorylceramide synthase (IPCS), an
296 enzyme involved in the metabolism of sphingolipids (Bromley et al 2003, Mandala et al 1998). The loss
297 of function of an IPCS gene in *Arabidopsis* has been shown to be associated with programmed cell
298 death linked to defence mechanisms (König et al 2021, Luttgeharm et al 2015, Ternes et al 2011, Wang
299 et al 2008, Zeng et al 2022, Zienkiewicz et al 2020). Given that the inhibition of plant IPCS can trigger
300 SA-dependent HR-like lesions, such as those observed in response to AgN23 CME, we decided to study
301 the implication of galbonolides in *Arabidopsis* responses to AgN23 (Vergnes et al 2020). We
302 constructed AgN23 knock out mutants in the polyketide synthase of the galbonolides BGCs by
303 disrupting the *gbnB* gene (AS97_41300) (Figure 4a). Galbonolides detection was fully abolished in the

304 CME of galbonolides knock-out mutants (Figure 4b). This finding confirmed the function of the
305 predicted galbonolide gene cluster in the synthesis of all the galbonolides detected (galbonolides A,
306 B, E and G).

307 To investigate the effect of AgN23 and galbonolide mutants CMEs on the IPCS activity, we prepared a
308 microsomal fraction from a *Saccharomyces cerevisiae* strain producing recombinant *Arabidopsis* IPCS2
309 (AT2G37940)(Pinneh et al 2019) and IPCS enzymatic activity was tracked by HPLC-Fluorescence
310 method with the fluorescent substrate NBD-C6-ceramide (Zhong et al 1999). Data were fitted to the
311 Michaelis-Menten equation and the apparent Km and Vmax were estimated to be 7.57µM and
312 0.01mol.min^{-1}.mg^{-1} of protein, respectively (Pinneh et al 2019)(Supplementary Figure S4).

313 We then tested the enzymatic activity in presence of AgN23 and mutant CMEs in the concentration
314 range of 100– 300µg/ml. We observed that the AgN23 CME displayed a drastic inhibition of the
315 enzymatic activity at concentrations greater than 200µg/ml dilution (Figure 4c) whereas no such
316 inhibition was observed in the CME of two selected AgN23 galbonolides knock-out mutants (Δ*gbnB-2*
317 and Δ*gbnB-4*). Taken together, these data revealed that galbonolides secretion by AgN23 is the driving
318 factor in the inhibition of *Arabidopsis* IPCS2.
319 Complementarily, since galbonolides were originally described as antifungal metabolites, the
320 antifungal activity of the mutant was analysed against the filamentous fungus *Botrytis cinerea* (Harris
321 et al 1998, Takatsu et al 1985). As expected, the loss of galbonolides in knock out mutants resulted in
322 a reduced antifungal activity of the CME (Supplementary Figure S5, Table 2).

323 **Galbonolides are major contributors of the AgN23 eliciting activity and play a crucial role in**
324 **rhizosphere colonisation by AgN23**

325 In a previous work, we identified AgN23 as a *Streptomyces* strain producing strong elicitors of the
326 hypersensitive reaction (HR) including localised necrosis and expression of defence markers such as
327 *Pathogenesis Related 1 PR1)*, *Phytoalexin Deficient 4 (PAD4)* and *Phytoalexin Deficient 3*
328 *(PAD3*)(Vergnes et al 2020). Here, we investigated whether galbonolides may play important role in

329 these responses to the bacterium. Agroinfiltration of *Nicotiana benthamiana* leaves with AgN23 CME
330 induced cell death at 50 µg/ml concentration whereas no sign of necrosis could be observed at the
331 same concentration with CMEs of the galbonolides mutants Δ*gbnB-2* and Δ*gbnB-4* (Figure 5a). It is
332 noteworthy that similar necrotic responses were observed when CME of the wild type and mutant
333 strains were infiltrated at 200 µg/ml or higher concentrations, suggesting that other necrotic elicitors
334 were produced by the mutants. To investigate the effect of AgN23 CME on the necrotic responses of
335 *Arabidopsis*, we performed ion leakage assays from infiltrated leaf discs of *Arabidopsis* with the 4
336 independent mutants of AgN23 and further confirmed the reduction in necrotic responses triggered
337 by AgN23 when galbonolides biosynthesis is abolished (Figure 5b). As variation of nuclear calcium
338 concentration is a typical signal associated with HR, we analysed the nuclear calcium concentration of
339 *Arabidopsis* plants following treatment using a line expressing a nuclear apo-aequorin reporter gene.
340 This reporter line was also selected based on a previous observation that a nuclear calcium signal
341 controls the apoptotic cell death induced by d-*erythro*-sphinganine, a compound related to the
342 sphingolipid pathway, in tobacco cells (Lachaud et al 2010). Luminescence quantification triggered by
343 AgN23 CME in hydroponically grown *Arabidopsis* peaked at 4 minutes post treatment and this
344 signature was abolished in the galbonolides mutants (Figure 5c). Similarly, we analysed by live imaging
345 *Arabidopsis* seedlings inoculated at the root tip with AgN23 CME and observed that this treatment
346 resulted in a quick activation (<15 min) of nuclear calcium signalling in the root tip which then spread
347 to the entire root plantlets (Supplementary Movie).

348 To investigate the impact of galbonolides production on root development, *in vitro* grown seedlings
349 were inoculated with galbonolides mutants and no root growth inhibition was observed with the two
350 mutants (Figure 6a and 6b). Furthermore, the robust induction of expression in *PR1*, *PAD3,* and *PAD4*
351 by AgN23 CME was compromised when using the 4 galbonolides KO mutants (Figure 6c). Thus, our
352 data prove that galbonolides are required for the activation of immune gene expression in *Arabidopsis*
353 seedlings in response to AgN23.

354 In view of our finding that *Arabidopsis* responds to AgN23 by strongly activating camalexin
355 biosynthesis, we studied the effect of *in vitro* spore inoculation of Col-0 with AgN23 and the two
356 galbonolide mutants Δ*gbnB-2* and Δ*gbnB-4*, by LC-HRMS metabolic fingerprinting (Supplementary
357 Table S4). The PCA revealed a significant difference in the metabolome response to the two AgN23
358 mutants as compared to the wild type (Figure 6d). Strikingly, the induction of camalexin detection was
359 significantly lower in roots inoculated with galbonolides mutants as compared to the wild type
360 bacterium (Figure 6e).

361 Soil inoculation with galbonolides mutants did not resulted in the reduced growth of Col-0 rosette
362 triggered by the wild-type bacteria (Figure 6f, 6g). In addition, Col-0 rhizosphere colonisation by
363 galbonolides mutants was reduced by contrast with wild type AgN23 (Figure 6h). Put together, these
364 data clearly point to the crucial role played by galbonolides for the induction of plant responses as
365 well as the ability of the bacterium to colonise the rhizosphere.

366 **DISCUSSION**

367 Understanding the chemical basis of the communication between plants and their associated
368 microorganisms is essential to improve the function and composition of plant microbiota, notably in
369 the context of developing sustainable agriculture practices. Towards this effort, *Streptomyces* species
370 could play a major role due to their ability to efficiently colonize the rhizospheric niche and to produce
371 a wide array of specialized metabolites with various biological activity. However, mechanisms involved
372 in the establishment and long-term maintenance of active microbial strains in the rhizosphere are
373 largely unknown.

374 To gain insight into these mechanisms we focussed on a *Streptomyces* strain, AgN23, initially isolated
375 from the grape rhizosphere and that efficiently colonizes the rhizosphere of *A. thaliana*. Metabolic
376 fingerprinting of the *Arabidopsis* response to AgN23 revealed that the response is mainly
377 characterised by the production of camalexin, which is the primary *Arabidopsis* phytoalexin involved
378 in resistance to fungal pathogens but also in the regulation of root microbiota composition and the

379 recruitment of PGPRs (Koprivova et al 2019, Koprivova et al 2023, Nguyen et al 2022). The use of *pad3-*
380 *1* camalexin deficient mutant of *Arabidopsis* demonstrated that the efficient colonization of the
381 rhizosphere by AgN23 relies on the production of this compound. While camalexin is an antimicrobial
382 compound, the *pad3-1* mutants did not show any signs of over colonisation by AgN23, suggesting that
383 camalexin does not act as an inhibitor of AgN23 development but, on the reverse, favours colonisation
384 of the rhizosphere by AgN23. Albeit camalexin is produced in response to a number of bacterial and
385 fungal phytopathogens, this does not mean it is biologically active against these microorganisms
386 (Glawischnig et al, 2007). It was reported that concentrations up to 500 $\mu g.ml^{-1}$ are required to achieve
387 membrane disruption in Gram negative bacteria, a range of concentration unlikely to be observed in
388 or around *Arabidopsis* roots (Rogers et al, 1996). By contrast fungal colonisers of plant roots are
389 sensitives to lower doses of camalexin (Rogers et al, 1996). Thus, the precise role of camalexin in
390 supporting the development of AgN23 in the rhizosphere remains to be elucidated, but it can be
391 hypothesized that camalexin can reduce the proliferation of susceptible fungi increasing available
392 nutritional resources for AgN23. Recently, it has been shown that camalexin, and more generally
393 tryptophan-derived metabolites, has been shown to be essential to prevent fungal dysbiosis in the
394 *Arabidopsis* rhizosphere (Wolinska et al 2021).

395 To understand the molecular mechanisms underlying the induction of camalexin biosynthesis by
396 AgN23, we investigated the composition of the bacteria exometabolome using untargeted
397 metabolomic tools. This analysis identied several specialised compounds with known antimicrobial
398 activity and for some of them, a putative function in eliciting plant defences. Among these compounds,
399 we decided to delve into the role of galbonolides in AgN23's biological activities, since it has been
400 shown that galbonolides target the sphingolipid metabolism by inhibiting the Inositol
401 Phosphorylceramide Synthase (IPCS) in both plants and fungi (Bromley et al 2003, Mandala et al 1998).
402 Sphingolipids are signalling molecules known to play a major role in plant defence (Berkey et al 2012),
403 notably for the activation of camalexin biosynthesis (Zienkiewicz et al 2020). Fungal toxins acting on
404 this metabolism such as Fumonisin B1, an inhibitor of ceramide synthase produced by pathogenic

405 *Fusarium* sp. may result in locally modifying the ceramide composition leading to induction of a
406 hypersensitive response (Iqbal et al 2021, Zeng et al 2020). To investigate the role of galbonolides in
407 the induction of plant defences by AgN23 we produced galbonolide mutants through the disruption
408 of a single BGC, confirming earliest reports indicating that all galbonolide variants are produced
409 through a single BGC (Karki et al 2010, Kim et al 2014, Liu et al 2015a, Liu et al 2015b). Using these
410 mutants we performed a set of complementary experiments which pointed to the major requirement
411 of galbonolides to trigger plant responses to AgN23 colonization.

412 Importantly, the lack of enrichment of galbonolide mutants in the *Arabidopsis* rhizosphere shows that
413 induction of plant defence by these compounds are beneficial for the AgN23 rhizospheric lifestyle. The
414 connections between plant immune responses and stimulation of root microorganisms has been
415 recently exemplified (Harbort et al 2020, Singh et al 2023, Stringlis et al 2018a, Voges et al 2019). For
416 example, the Plant Growth Promoting Rhizobacteria (PGPR) *Pseudomonas* sp. CH267 triggers the
417 production of camalexin (Koprivova et al 2019, Koprivova et al 2023). Similarly, *Arabidopsis* root
418 inoculation with the proteobacteria *Pseudomonas simiae* WCS417 results in the secretion of
419 scopoletin, a coumarin that facilitates *P. simiae* root colonisation while inhibiting the growth of fungal
420 pathogens and diverse other bacterial taxa (Stringlis et al 2018b).

421 However, to our knowledge, the role of a specific microbial compound in eliciting plant defense
422 responses for the benefit of the microganism has not yet been described and this result raises an
423 interesting question about the generality of the role of galbonolides in the rhizospheric microbiota.
424 While IPCS and the role of sphingolipid metabolism in immune responses are ubiquitous in plants, the
425 distribution of the galbonolide in the *Streptomyces* genus, and more generally in actinomycetes,
426 remains to be precised. In our previous study we showed that the galbonolide biosynthetic gene
427 cluster (BGC) is present in several species across the *S. violaceusniger* clade, to whom AgN23 belongs,
428 which includes several rhizospheric isolates (Gayrard et al 2023). In addition, the fact that galbonolides
429 were initially found in *S. galbus* which does not belong to the *S. violacesuniger* clade and in the

430 distantly related actinomycete *Micromonospora spp.* suggests that the biosynthesis of galbonolides
431 may be widespread across actinomycete representatives (Achenbach et al 1988, Karki et al 2010, Kim
432 et al 2014, Shaffie et al 2001, Sigmund et al 1998). Further studies will aim to evaluate the impact of
433 galbonolide production of microbiota functioning through the direct antifungal activity of these
434 compounds and their impact on the production plant anti-fungal metabolites.

435 **DATA AVAILIBILITY**

436 Datasets generated or analyzed during this study are included in this published article (and its
437 Supplementary Table files). Raw data regarding RNAseq analysis and their complete analysis can be
438 found on the NCBI Gene Expression Omnibus (GSE119986)(Vergnes et al 2020). The genome assembly
439 of AgN23 is available on the NCBI "Nucleotide" repository (NZ_CP007153.1) with the chromosome
440 sequence and the automatic annotation pipeline used to define gene models (Gayrard et al 2023). The
441 LC-HRMS chromatograms of AgN23 CME and *Arabidopsis* are available on Zenodo repository
442 (8421008).

443 **ACKNOWLEDGEMENTS**

444 We thank Dr. Paul Denny (Warwick University) for sharing the yeast line that allowed to purify
445 microsomal fractions bearing *AtIPCS2,* and Dr. Pawel Bednarek for the *pad3-1* seeds. We thank Dr.
446 Revathi Bacsa for her help in the writing of the manuscript.

447 **AUTHOR CONTRIBUTIONS**

448 Clément Nicolle, Damien Gayrard, Alba Noël, Marion Hortala, Guillaume Marti, Aurélien Amiel, Sabine
449 Grat and Aurélie Le Ru performed the research. Clément Nicolle, Jean-Luc Pernodet, Sylvie Lautru,
450 Bernard Dumas and Thomas Rey wrote the paper.

451 **DECLARATION OF INTERESTS**

452 The following information may be seen as competing interests. B.D. is one of the inventors of the
453 patent WO2015044585A1 related to the use of AgN23 in agriculture. T.R. and D.G. are full-time

researchers at the AgChem company De Sangosse (Pont-Du-Casse, France), which registers and markets crop-protection products and owns the patent WO2015044585A1.

FUNDING

This work was funded by the Fond Unique Interministériels (NEOPROTEC project), the Fonds Européen de Développement Économique et Régional (FEDER), the Agence Nationale de la Recherche (LabCom BioPlantProtec ANR-14-LAB7-0001 and STREPTOCONTROL ANR-17-CE20-0030), and the Région Occitanie (projet GRAINE-BioPlantProducts). Thewpork carried out at the Metatoul-AgromiX Platform was peformed in the frame of MetaboHUB-ANR-11-INBS-0010. The Laboratoire de Recherche en Sciences Végétales (LRSV) belongs to the TULIP Laboratoire d'Excellence (ANR-10-LABX-41) and benefits from the "École Universitaire de Recherche (EUR)" TULIP-GS (ANR-18-EURE-0019). Work performed in the GeT core facility, Toulouse, France (https://get.genotoul.fr) was supported by the France Génomique National infrastructure, funded as part of the "Investissement d'Avenir" program managed by the Agence Nationale de la Recherche (contract ANR-10-INBS-09) and by the GET-PACBIO program (FEDER Programme opérationnel FEDER-FSE MIDI-PYRENEES ET GARONNE 2014-2020). D. Gayrard was funded by the Agence Nationale de la Recherche Technique, with the « Convention Industrielle de Formation par la Recherche and Association Nationale de la Recherche et de la Technologie » (Grant N° 2016/1297). C. Nicolle was funded by the Ministère de l'Enseignement Supérieur et de la Recherche (PhD fellowship).

REFERENCE

Achenbach H, Mühlenfeld A, Fauth U, Zähner H (1988). The galbonolides. Novel, powerful antifungal macrolides from *Streptomyces galbus* ssp. eurythermus. *Ann N Y Acad Sci* **544:** 128-140.

Andrić S, Meyer T, Rigolet A, Prigent-Combaret C, Höfte M, Balleux G *et al* (2021). Lipopeptide Interplay Mediates Molecular Interactions between Soil *Bacilli* and *Pseudomonads*. *Microbiol Spectr* **9:** e0203821.

Andrić S, Rigolet A, Argüelles Arias A, Steels S, Hoff G, Balleux G *et al* (2023). Plant-associated *Bacillus* mobilizes its secondary metabolites upon perception of the siderophore pyochelin produced by a *Pseudomonas* competitor. *ISME J* **17:** 263-275.

481 Avalos M, Garbeva P, Raaijmakers JM, van Wezel GP (2020). Production of ammonia as a low-cost and
482 long-distance antibiotic strategy by *Streptomyces* species. *ISME J* **14:** 569-583.

483

484 Berendsen RL, Vismans G, Yu K, Song Y, de Jonge R, Burgman WP *et al* (2018). Disease-induced
485 assemblage of a plant-beneficial bacterial consortium. *ISME J* **12:** 1496-1507.

486 Berkey R, Bendigeri D, Xiao S (2012). Sphingolipids and Plant Defense/Disease: The "Death"
487 Connection and Beyond. *Frontiers in Plant Science* **3:** 68.

488 Bromley PE, Li YO, Murphy SM, Sumner CM, Lynch DV (2003). Complex sphingolipid synthesis in plants:
489 characterization of inositolphosphorylceramide synthase activity in bean microsomes. *Arch Biochem*
490 *Biophys* **417:** 219-226.

491 Bulgarelli D, Rott M, Schlaeppi K, Ver Loren van Themaat E, Ahmadinejad N, Assenza F *et al* (2012).
492 Revealing structure and assembly cues for *Arabidopsis* root-inhabiting bacterial microbiota. *Nature*
493 **488:** 91-95.

494 Busby PE, Soman C, Wagner MR, Friesen ML, Kremer J, Bennett A *et al* (2017). Research priorities for
495 harnessing plant microbiomes in sustainable agriculture. *PLoS Biol* **15:** e2001793.

496 Cha JY, Han S, Hong HJ, Cho H, Kim D, Kwon Y *et al* (2016). Microbial and biochemical basis of a
497 Fusarium wilt-suppressive soil. *ISME J* **10:** 119-129.

498 Chaparro JM, Badri DV, Vivanco JM (2014). Rhizosphere microbiome assemblage is affected by plant
499 development. *ISME J* **8:** 790-803.

500 Conn VM, Walker AR, Franco CM (2008). Endophytic actinobacteria induce defense pathways in
501 *Arabidopsis thaliana*. *Mol Plant Microbe Interact* **21:** 208-218.

502 Cordovez V, Carrion VJ, Etalo DW, Mumm R, Zhu H, van Wezel GP *et al* (2015). Diversity and functions
503 of volatile organic compounds produced by *Streptomyces* from a disease-suppressive soil. *Front*
504 *Microbiol* **6:** 1081.

505 Durán P, Thiergart T, Garrido-Oter R, Agler M, Kemen E, Schulze-Lefert P *et al* (2018). Microbial
506 Interkingdom Interactions in Roots Promote *Arabidopsis* Survival. *Cell* **175:** 973-983.e914.

507

508 Fitzpatrick CR, Copeland J, Wang PW, Guttman DS, Kotanen PM, Johnson MTJ (2018). Assembly and
509 ecological function of the root microbiome across angiosperm plant species. *Proc Natl Acad Sci U S A*
510 **115:** E1157-E1165.

511 Fitzpatrick CR, Salas-González I, Conway JM, Finkel OM, Gilbert S, Russ D *et al* (2020). The Plant
512 Microbiome: From Ecology to Reductionism and Beyond. *Annu Rev Microbiol* **74:** 81-100.

513 Gayrard D, Nicolle C, Veyssière M, Adam K, Martinez Y, Vandecasteele C *et al* (2023). Genome
514 Sequence of the *Streptomyces* Strain AgN23 Revealed Expansion and Acquisition of Gene Repertoires
515 Potentially Involved in Biocontrol Activity and Rhizosphere Colonization. *PhytoFrontiers* **3(3):** 535-547.

516 Getzke F, Hassani MA, Crüsemann M, Malisic M, Zhang P, Ishigaki Y *et al* (2023). Cofunctioning of
517 bacterial exometabolites drives root microbiota establishment. *Proceedings of the National Academy*
518 *of Sciences* **120:** e2221508120.

519 Glawischnig, E. (2007). Camalexin. Phytochemistry, **68**: 401-406.

520

521 Harbort CJ, Hashimoto M, Inoue H, Niu Y, Guan R, Rombolà AD *et al* (2020). Root-Secreted Coumarins
522 and the Microbiota Interact to Improve Iron Nutrition in *Arabidopsis*. *Cell Host & Microbe* **28(6):** 825-
523 837.

Harris GH, Shafiee A, Cabello MA, Curotto JE, Genilloud O, Göklen KE *et al* (1998). Inhibition of fungal sphingolipid biosynthesis by rustmicin, galbonolide B and their new 21-hydroxy analogs. *J Antibiot (Tokyo)* **51:** 837-844.

Iqbal N, Czékus Z, Poór P, Ördög A (2021). Plant defence mechanisms against mycotoxin Fumonisin B1. *Chem Biol Interact* **343:** 109494.

Karki S, Kwon SY, Yoo HG, Suh JW, Park SH, Kwon HJ (2010). The methoxymalonyl-acyl carrier protein biosynthesis locus and the nearby gene with the beta-ketoacyl synthase domain are involved in the biosynthesis of galbonolides in *Streptomyces galbus*, but these loci are separate from the modular polyketide synthase gene cluster. *FEMS Microbiol Lett* **310:** 69-75.T. Kieser, M. J. Bibb, M. J. Buttner, K. K. Chater, D. A. Hopwood, Practical streptomyces genetics (John Innes Foundation, 2000).

Kim DR, Cho G, Jeon CW, Weller DM, Thomashow LS, Paulitz TC *et al* (2019). A mutualistic interaction between *Streptomyces* bacteria, strawberry plants and pollinating bees. *Nat Commun* **10:** 4802.

Kim HJ, Karki S, Kwon SY, Park SH, Nahm BH, Kim YK *et al* (2014). A single module type I polyketide synthase directs de novo macrolactone biogenesis during galbonolide biosynthesis in *Streptomyces galbus*. *J Biol Chem* **289:** 34557-34568.

Koprivova A, Schuck S, Jacoby RP, Klinkhammer I, Welter B, Leson L *et al* (2019). Root-specific camalexin biosynthesis controls the plant growth-promoting effects of multiple bacterial strains. *Proceedings of the National Academy of Sciences* **116:** 15735-15744.

Koprivova A, Schwier M, Volz V, Kopriva S (2023). Shoot-root interaction in control of camalexin exudation in *Arabidopsis*. *J Exp Bot* **74:** 2667-2679.

Krespach MKC, Stroe MC, Flak M, Komor AJ, Nietzsche S, Sasso S *et al* (2021). Bacterial marginolactones trigger formation of algal gloeocapsoids, protective aggregates on the verge of multicellularity. *Proceedings of the National Academy of Sciences* **118:** e2100892118.

Krespach MKC, Stroe MC, Netzker T, Rosin M, Zehner LM, Komor AJ *et al* (2023). *Streptomyces* polyketides mediate bacteria–fungi interactions across soil environments. *Nature Microbiology* **8:** 1348-1361.

Kurth F, Mailänder S, Bönn M, Feldhahn L, Herrmann S, Große I *et al* (2014). *Streptomyces*-induced resistance against oak powdery mildew involves host plant responses in defense, photosynthesis, and secondary metabolism pathways. *Mol Plant Microbe Interact* **27:** 891-900.

König S, Gömann J, Zienkiewicz A, Zienkiewicz K, Meldau D, Herrfurth C *et al* (2021). Sphingolipid-Induced Programmed Cell Death is a Salicylic Acid and *EDS1*-Dependent Phenotype in Arabidopsis fatty acid hydroxylase *(fah1, fah2*) and ceramide synthase (*loh2*) Triple Mutants. *Plant Cell Physiol* **63(3)**: 317-325.

Lachaud C, Da Silva D, Cotelle V, Thuleau P, Xiong TC, Jauneau A *et al* (2010). Nuclear calcium controls the apoptotic-like cell death induced by d-erythro-sphinganine in tobacco cells. *Cell Calcium* **47:** 92-100.

Lebeis SL, Paredes SH, Lundberg DS, Breakfield N, Gehring J, McDonald M *et al* (2015). PLANT MICROBIOME. Salicylic acid modulates colonization of the root microbiome by specific bacterial taxa. *Science* **349:** 860-864.

Ling, N., Wang, T., & Kuzyakov, Y. (2022). Rhizosphere bacteriome structure and functions. Nature communications, **1**: 836-849.

Liu C, Zhang J, Lu C, Shen Y (2015a). Heterologous expression of galbonolide biosynthetic genes in *Streptomyces coelicolor*. *Antonie van Leeuwenhoek* **107:** 1359-1366.

567 Liu C, Zhu J, Li Y, Zhang J, Lu C, Wang H *et al* (2015b). In Vitro Reconstitution of a PKS Pathway for the
568 Biosynthesis of Galbonolides in *Streptomyces* sp. LZ35. *ChemBioChem* **16:** 998-1007.

569 Lundberg DS, Lebeis SL, Paredes SH, Yourstone S, Gehring J, Malfatti S *et al* (2012). Defining the core
570 *Arabidopsis thaliana* root microbiome. *Nature* **488:** 86-90.

571 Luttgeharm KD, Chen M, Mehra A, Cahoon RE, Markham JE, Cahoon EB (2015). Overexpression of
572 *Arabidopsis* Ceramide Synthases Differentially Affects Growth, Sphingolipid Metabolism, Programmed
573 Cell Death, and Mycotoxin Resistance. *Plant Physiol* **169:** 1108-1117.

574 Mandala SM, Thornton RA, Milligan J, Rosenbach M, Garcia-Calvo M, Bull HG *et al* (1998). Rustmicin,
575 a potent antifungal agent, inhibits sphingolipid synthesis at inositol phosphoceramide synthase. *J Biol*
576 *Chem* **273:** 14942-14949.

577 Mendes R, Raaijmakers JM (2015). Cross-kingdom similarities in microbiome functions. *The ISME*
578 *Journal* **9:** 1905-1907.

579 Mina JG, Okada Y, Wansadhipathi-Kannangara NK, Pratt S, Shams-Eldin H, Schwarz RT *et al* (2010).
580 Functional analyses of differentially expressed isoforms of the *Arabidopsis* inositol
581 phosphorylceramide synthase. *Plant Mol Biol* **73:** 399-407.

582

583 Nguyen NH, Trotel-Aziz P, Clément C, Jeandet P, Baillieul F, Aziz A (2022). Camalexin accumulation as
584 a component of plant immunity during interactions with pathogens and beneficial microbes. *Planta*
585 **255:** 116.

586 Pinneh EC, Mina JG, Stark MJR, Lindell SD, Luemmen P, Knight MR *et al* (2019). The identification of
587 small molecule inhibitors of the plant inositol phosphorylceramide synthase which demonstrate
588 herbicidal activity. *Sci Rep* **9:** 8083.

589 Rey T, Dumas B (2017). Plenty Is No Plague: *Streptomyces* Symbiosis with Crops. *Trends Plant Sci* **22:**
590 30-37.

591 Rogers, E. E., Glazebrook, J., & Ausubel, F. M. (1996). Mode of action of the Arabidopsis thaliana
592 phytoalexin camalexin and its role in Arabidopsis-pathogen interactions. Molecular Plant Microbe
593 Interactions, **9:** 748-757.

594 Russ D, Fitzpatrick CR, Teixeira PJPL, Dangl JL (2023). Deep discovery informs difficult deployment in
595 plant microbiome science. *Cell* **186:** 4496-4513.J. Sambrook, D. Russell, Molecular Cloning: A
596 Laboratory Manual, 3rd Revised edition (Cold Spring Harbor Laboratory Press,U.S., 2000).

597 Schuhegger R, Nafisi M, Mansourova M, Petersen BL, Olsen CE, Svatoš A *et al* (2006). CYP71B15 (PAD3)
598 Catalyzes the Final Step in Camalexin Biosynthesis. *Plant Physiology* **141:** 1248-1254.

599 Shafiee A, Harris G, Motamedi H, Rosenbach M, Chen T, Zink D *et al* (2001). Microbial hydroxylation
600 of rustmicin (galbonolide A) and galbonolide B, two antifungal products produced by *Micromonospora*
601 sp. *Journal of Molecular Catalysis B: Enzymatic* **11:** 237-242.

602 Sigmund JM, Hirsch CF (1998). Fermentation studies of rustmicin production by a *Micromonospora* sp.
603 *J Antibiot (Tokyo)* **51:** 829-836.

604 Singh G, Agrawal H, Bednarek P (2023). Specialized metabolites as versatile tools in shaping plant–
605 microbe associations. *Molecular Plant* **16:** 122-144.

606 Stringlis IA, Proietti S, Hickman R, Van Verk MC, Zamioudis C, Pieterse CMJ (2018a). Root
607 transcriptional dynamics induced by beneficial rhizobacteria and microbial immune elicitors reveal
608 signatures of adaptation to mutualists. *Plant J* **93:** 166-180.

609 Stringlis IA, Yu K, Feussner K, de Jonge R, Van Bentum S, Van Verk MC *et al* (2018b). MYB72-dependent
610 coumarin exudation shapes root microbiome assembly to promote plant health. *Proceedings of the*
611 *National Academy of Sciences* **115:** E5213-E5222.

612 Ternes P, Feussner K, Werner S, Lerche J, Iven T, Heilmann I *et al* (2011). Disruption of the ceramide
613 synthase LOH1 causes spontaneous cell death in *Arabidopsis thaliana*. *New Phytologist* **192:** 841-854.

614 Thiergart T, Durán P, Ellis T, Vannier N, Garrido-Oter R, Kemen E *et al* (2020). Root microbiota assembly
615 and adaptive differentiation among European *Arabidopsis* populations. *Nat Ecol Evol* **4:** 122-131.

616 Vergnes MS, Gayrard MD, Veyssiere MM, Toulotte MJ, Martinez MY, Dumont DV *et al* (2020).
617 Phyllosphere colonisation by a soil *Streptomyces* sp. promotes plant defense responses against fungal
618 infection. Molecular Plant-Microbe Interactions, **33(2):** 223-234.

619 Viaene T, Langendries S, Beirinckx S, Maes M, Goormachtig S (2016). *Streptomyces* as a plant's best
620 friend? *FEMS Microbiol Ecol* **92**.

621 Voges MJEEE, Bai Y, Schulze-Lefert P, Sattely ES (2019). Plant-derived coumarins shape the
622 composition of an *Arabidopsis* synthetic root microbiome. *Proceedings of the National Academy of*
623 *Sciences* **116:** 12558-12565.

624 Wang W, Yang X, Tangchaiburana S, Ndeh R, Markham JE, Tsegaye Y *et al* (2008). An
625 inositolphosphorylceramide synthase is involved in regulation of plant programmed cell death
626 associated with defense in *Arabidopsis*. *Plant Cell* **20:** 3163-3179.

627 Wolinska KW, Vannier N, Thiergart T, Pickel B, Gremmen S, Piasecka A *et al* (2021). Tryptophan
628 metabolism and bacterial commensals prevent fungal dysbiosis in *Arabidopsis* roots. *Proceedings of*
629 *the National Academy of Sciences* **118:** e2111521118.

630 Yang Z, Qiao Y, Konakalla NC, Strøbech E, Harris P, Peschel G *et al* (2023). *Streptomyces* alleviate abiotic
631 stress in plant by producing pteridic acids. *Nature Communications* **14:** 7398.

632 Zeng H-Y, Bao H-N, Chen Y-L, Chen D-K, Zhang K, Liu S-K *et al* (2022). The Two Classes of Ceramide
633 Synthases Play Different Roles in Plant Immunity and Cell Death. *Frontiers in Plant Science* **13:** 824585.

634 Zeng HY, Li CY, Yao N (2020). Fumonisin B1: A Tool for Exploring the Multiple Functions of Sphingolipids
635 in Plants. *Front Plant Sci* **11:** 600458.

636 Zhong W, Murphy DJ, Georgopapadakou NH (1999). Inhibition of yeast inositol phosphorylceramide
637 synthase by aureobasidin A measured by a fluorometric assay. *FEBS Letters***:** 4.

638 Zienkiewicz A, Gömann J, König S, Herrfurth C, Liu YT, Meldau D *et al* (2020). Disruption of *Arabidopsis*
639 neutral ceramidases 1 and 2 results in specific sphingolipid imbalances triggering different
640 phytohormone-dependent plant cell death programmes. *New Phytol* **226:** 170-188.

641

642

643

644

645

TABLE

Table 1: List of detected metabolites with highest intensities on chromatogram

Peak name	Ret. Time (min)	m/z
Galbonolide E	7.63	365.19
Galbonolide A	7.92	379.21
Galbonolide G	8.21	363.21
Niphimycin	8.53	1140.71
Niphimycin	9.15	1140.71
Nigericin	12.41	723.47
Nigericin	15.12	723.47

Table 2: 50% inhibitory concentration (IC_{50}) of AgN23 WT and KO mutants (Δ*gbnB*) CME against *Botrytis cinerea.* Table shows mean ± SD calculated from six biological replicates (n = 6)

Strain	IC_{50} (µg/mL)
AgN23 WT	33.28 ± 0.20
ΔgbnB-1	48.06 ± 1.68
Δ*gbnB-2*	47.27 ± 1.29
Δ*gbnB-3*	46.13 ± 1.29
Δ*gbnB-4*	54.42 ± 3.7

FIGURE LEGENDS

Figure 1: AgN23 colonizes rhizoplane and rhizosphere of *Arabidopsis thaliana* and slightly inhibits plant growth. a. Observation of *A. thaliana* Col-0 colonization by AgN23 at 10 days after inoculation with spores at the root apex. Arrowheads indicate AgN23 initial spore inoculation, Scale bar = 1 cm. **b.** Confocal fluorescence images of AgN23-mCherry (red) colonizing root apical meristem and AgN23-GFP (green) developing around lateral root. Scale bars: 250µm **c.** Primary root length of *Arabidopsis* seedlings 10 days after inoculation with AgN23 spores at the root apex from Violin plots created from data from 30 independent assays each involving at least 10 plants per treatment (n = 300). The whiskers encompass the minimum and maximum values, and the midline shows the median. Statistical differences between the treatments were analyzed using Mann–Whitney test and '****' represents significant differences at *P* value < 0.0001. **d.** Typical photographs of 6-week- old Arabidopsis rosettes following growth within non- or inoculated potting soil. Scale bar: 1 cm. **e.** Leaf

664 area measurement of *Arabidopsis* rosettes grown in AgN23-inoculated potting soil. Graphs show the
665 mean ± SD calculated from at least eight biological replicates (n = 8). Statistical comparison between
666 inoculation and mock conditions was performed based on T-test ('**' = *P* value < 0.01; '***' = *P* value
667 < 0.001; '****' = *P* value < 0.0001). **f.** AgN23 genome copy number in *Arabidopsis* rhizosphere 4 and 8
668 weeks after soil inoculation. Box plots were created from data involving at least 8 plants per treatment
669 (n = 8). Whiskers encompass the minimum and maximum values, and the midline shows the median.
670 Statistical differences between the treatments were analyzed using Mann–Whitney test; '****' and
671 '**' represent significant differences at *P* value < 0.0001 and *P* value < 0.05, respectively.

672 **Figure 2: AgN23 induces camalexin biosynthesis in *Arabidopsis* roots. a. Discriminant metabolites**
673 **overrepresented in mock or AgN23 treated *Arabidopsis* roots based on UHPLC-MS profiling data.**
674 The metabolites are displayed as chemical classes, determined with Classyfire, using the criteria of *P*
675 value < 0.05 (T-test, control vs treatment, unadjusted *P* value) and log2 fold change (log2FC) > 0.8 or
676 < -0.8. **b.** Corresponding S-plot of OPLS-DA score plot based on Mock vs AgN23 comparison (n = 511
677 variables, the OPLS-DA model was validated by a permutation test with 200 counts). The variables
678 with VIP > 3.5 are indicated by orange and blue filled circles for AgN23 group and mock group,
679 respectively. c. Average peak area of the 2 biomarkers significantly induced in AgN23 treated roots
680 (VIP > 3.5). Box plots were created from data from six independent assays (n = 6). The whiskers
681 encompass the minimum and maximum values, and the midline shows the median. Statistical
682 differences between the treatments were analyzed using unpaired T-test and '**' represents
683 significant differences at *P* value < 0.01. I3M: indole-3-yl-methyl. **d.** PCA score plot of UHPLC-MS data
684 (n = 534 variables) from extracts of *Arabidopsis* Col-0 or *pad3-1* 10 days after inoculation with AgN23.
685 **e.** Average peak area of camalexin. Box plots were created from data from six independent assays (n
686 = 6). The whiskers encompass the minimum and maximum values, and the midline shows the median.

687 **Figure 3: Biosynthesis of camalexin enables enrichment of AgN23 in the *Arabidopsis* rhizosphere. a.**
688 Observation of *A. thaliana* Col-0 and *pad3-1* colonization by AgN23 at 10 days after inoculation with

689 spores at the root apex. Scale bar = 2 cm **b.** Rosette development of the plants Col-0 and *pad3-1* after
690 inoculation with AgN23 spores. Typical photographs of 6-week-old col-0 or pad3 rosettes are shown.
691 **c.** Primary root length of plants colonized or not by AgN23 at 10 days after inoculation. **d.** Leaf area
692 measurement. Graphs show the mean ± SD calculated from at least eight biological replicates (n = 8).
693 **e.** AgN23 genome copy number in Col-0 or *pad3-1 Arabidopsis* rhizosphere 6 weeks after soil
694 inoculation with AgN23. Box plots were created from data from 5 plants per treatment (n = 5). The
695 whiskers encompass the minimum and maximum values, and the midline shows the median. Letters
696 a to c represent statistical differences between the treatments based on 2-way ANOVA followed by
697 Tukey's multiple comparisons test.

698 **Figure 4: AgN23 produces galbonolides, a class of macrolides capable of inhibiting plant**
699 **Inositolphosphoryl Ceramide Synthase. a.** Biosynthesis pathway of galbonolides (*gbn*A-E) and of
700 methoxymalonyl-CoA (*gbn*H-K) in AgN23. The targeted locus of the AgN23 galbonolide BCG for knock-
701 out is shown by the red broken line (NCBI locus tags from assembly GCA_001598115.2). **b.** Average
702 peak area of the different putative galbonolides structures detected in AgN23 Culture Media Extract
703 based on HRMS and MS/MS spectra. Box plots were created from data from 6 biological replicates (n
704 = 6). The whiskers encompass the minimum and maximum values, and the midline shows the median.
705 Statistical differences between the AgN23 wild-type (WT) group and the AgN23 KO (Δ*gbnB*) groups
706 were analyzed using one-way analysis of variance (ANOVA) and Tukey's HSD test (α = 0.05) and '****'
707 represents significant differences at *P* value < 0.0001. **c.** Pathway of of NBD-C6-ceramide to NBD-C6-
708 IPC conversion by the *Arabidopsis* Inositolphosphoryl Ceramide Synthase (AtIPCS2) and enzyme
709 activity following treatments with butanol extracts from culture supernatant of AgN23 WT or KO
710 mutants (Δ*gbnB*-2 and Δ*gbnB-4*). Graphs show the mean ± SD calculated from 6 independent assays
711 (n = 6). Statistical differences between the AgN23 wild-type (WT) group and the AgN23 KO (Δ*gbnB*)
712 groups were analyzed using multiple Mann-Whitney test (FDR = 1%) and '***' and '**' represent *P*
713 value < 0.001 and *P* value < 0.01, respectively.

714 **Figure 5**: **The Culture Media Extract of AgN23 triggers a galbonolides dependent hypersensitive**
715 **response a.** Typical photographs of necrotic symptoms in *Nicotiana benthamiana* leaves 48h after
716 infiltration with CME of AgN23 WT or KO mutants (Δ*gbnB-2* and Δ*gbnB-4*) at 50, 100, 200 and 400
717 µg/mL as indicated in the scheme (n = 6). Scale bar: 3 cm. **b.** Ion leakage measurements of *Arabidopsis*
718 leaf disks infiltrated with CME of AgN23 WT or KO mutants (Δ*gbnB*) at 100 µg/mL. Box plots were
719 created with data from 6 independent assays involving 5 to 6 leaf disks (n = 6). The letters a–c indicate
720 statistically significant differences according to one-way analysis of variance (ANOVA) and Tukey's HSD
721 test (Honestly Significantly Different, α = 0.05). **c.** Kinetics of AgN23 or KO mutants CME-induced
722 nuclear calcium influxes in *Arabidopsis seedlings expressing* nuclear-localized aequorin. CME at 100
723 µg/mL was added at time = 0 min. Graphs show the mean ± SD calculated from 10 independent assays
724 involving 3 plants per treatment (n = 10).

725 **Figure 6: Galbonolides play a crucial role in defense gene activation, camalexin biosynthesis and**
726 **AgN23 persistence in the rhizosphere**. **a.** Observation of *Arabidopsis thaliana* Col-0 colonization by
727 AgN23 WT or KO mutants at 10 days after inoculation with spores at the root apex. Scale bar: 2 cm. **b.**
728 Primary root length of plants colonized by AgN23 WT or KO mutants (Δ*gbnB*) at 10 days after
729 inoculation. Statistical differences between the treatments were analyzed using Mann–Whitney test
730 and '****' represents significant differences at *P* value < 0.0001. **c.** Analysis of *PR1*, *PAD3*, and *PAD4*
731 defense gene expression in 10-day old *Arabidopsis* seedlings at 6 hours after treatment with AgN23
732 CME. Graphs show the mean $2^{-\Delta Cp}$ relative to *UBQ10* and SD calculated from three biological replicates
733 (n = 3), each involving five plants. Statistical comparisons were performed with T-test ('*' = *P* value <
734 0.05). **d.** PCA score plot of UHPLC-HRMS data (n = 256 variables) from extracts of *Arabidopsis thaliana*
735 10 days after inoculation with AgN23 WT or KO mutants (Δ*gbnB*) **E.** Average peak area of camalexin.
736 Box plots were created from data from six independent assays (n = 6). The whiskers encompass the
737 minimum and maximum values, and the midline shows the median. Statistical differences between
738 the treatments were analyzed using unpaired T-test and '****' represents significant differences at *P*
739 value < 0.0001.**f.** Typical photographs of 6-week-old Col-0 rosettes grown in potting soil inoculated

740 with AgN23 WT or KO mutants spores. Scale bar: 1.7 cm **g.** Leaf area measurement. Graphs show the
741 mean ± SD calculated from at least eight biological replicates (n = 8). **h.** AgN23 WT and Δ*gbnB-2* and
742 Δ*gbnB-4)* mutants genome copy number in Col-0 rhizosphere 6 weeks after soil inoculation. Box plots
743 were created from data from 8 plants per treatment (n = 8). The whiskers encompass the minimum
744 and maximum values, and the midline shows the median. The letters a–c represent statistical
745 differences between the treatments based on 2-way ANOVA followed by Tukey's multiple
746 comparisons test.

747 **Graphical Abstract: Model summarizing the mode of action of galbonolides in stimulating plant**
748 **defence to support AgN23 colonization of the rhizosphere.** Galbonolides secretion by *Streptomyces*
749 sp. AgN23 trigger Inositol Phosphoceramide Synthase (IPCS) inhibition in *Arabidopsis* root cells (orange
750 arrow). The resulting raise in Ceramide precursors of the IPCS may result in the different defence
751 responses associated to AgN23: Hypersensitive Responses (HR), Salicylic Acid (SA) signalling, nuclear
752 Ca^{2+} influx, defence gene expression and camalexin biosynthesis. This production of camalexin (blue
753 arrow) exert a positive effect on AgN23 growth in the rhizosphere, presumably by restricting the
754 growth of bacterial and fungal competitors sensitive to this phytoalexin. In addition, galbonolides
755 secretion in the rhizosphere may also directly interfere with fungal competitors of AgN23.

756

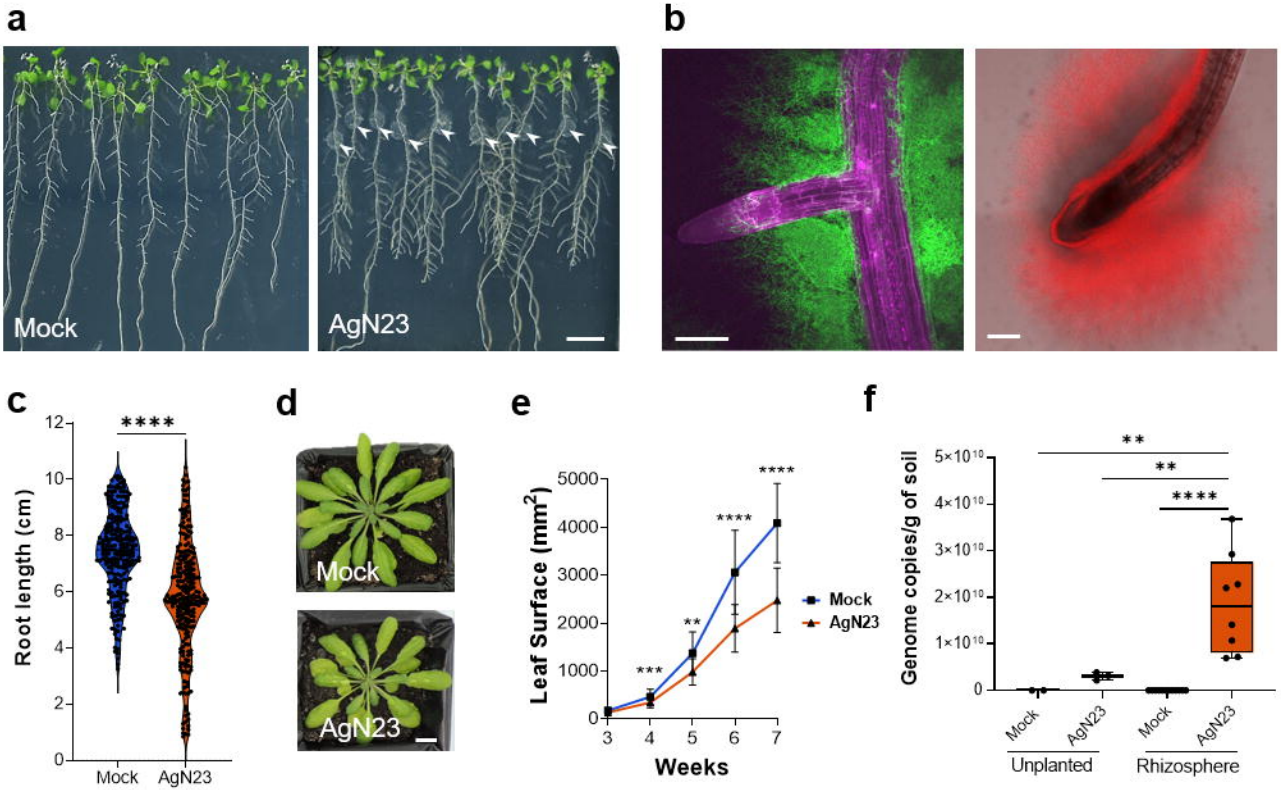
a
Mock
AgN23
b
c
****
Root length (cm)
Mock
AgN23
d
Mock
AgN23
e
Leaf Surface (mm²)
Weeks
Mock
AgN23
***
**
****
****
f
Genome copies/g of soil
Mock
AgN23
Mock
AgN23
Unplanted
Rhizosphere
**
**
****

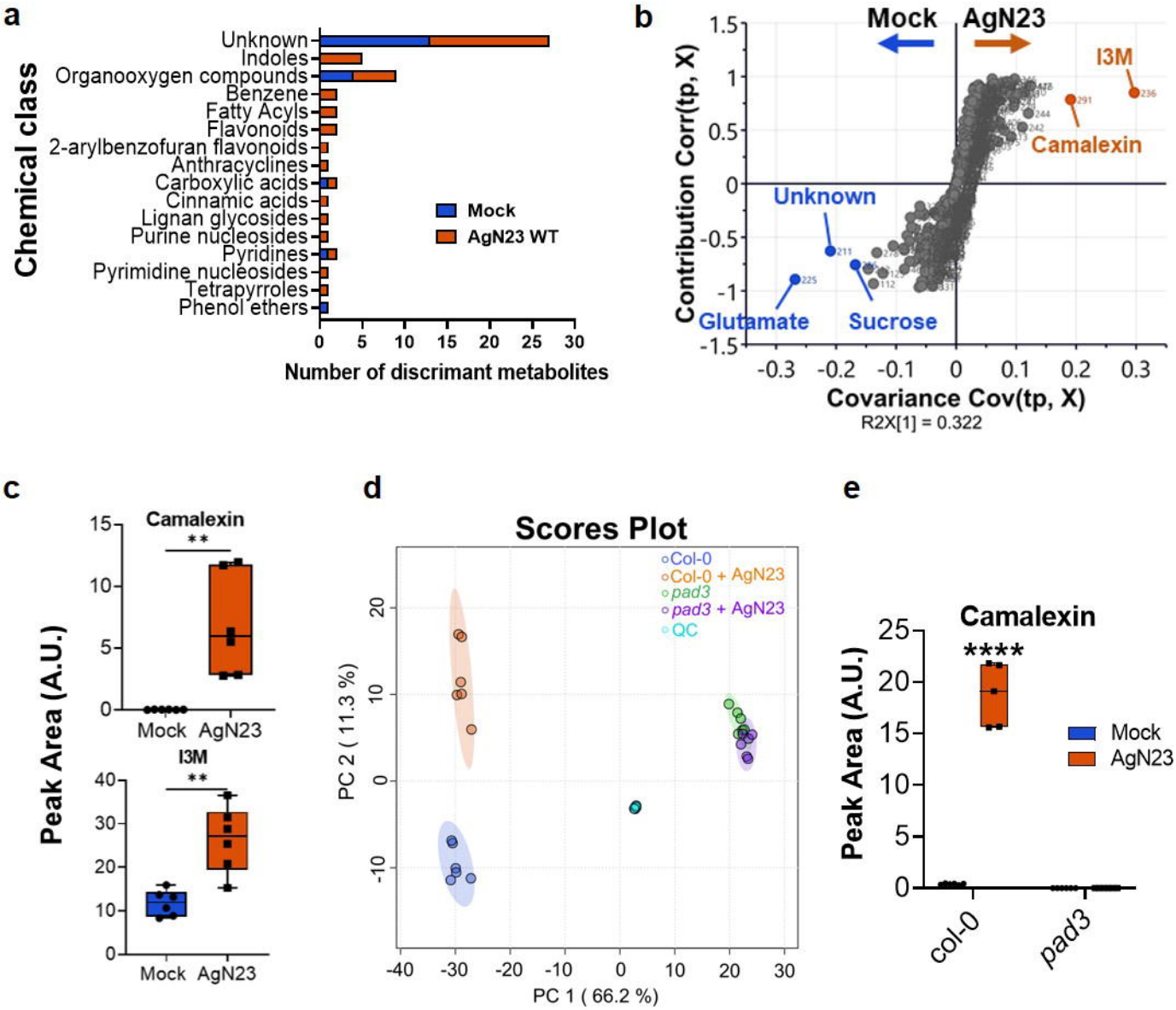
a
Chemical class
Unknown
Indoles
Organooxygen compounds
Benzene
Fatty Acyls
Flavonoids
2-arylbenzofuran flavonoids
Anthracyclines
Carboxylic acids
Cinnamic acids
Lignan glycosides
Purine nucleosides
Pyridines
Pyrimidine nucleosides
Tetrapyrroles
Phenol ethers
Mock
AgN23 WT
0 5 10 15 20 25 30
Number of discrimant metabolites
b
Mock
AgN23
I3M
Camalexin
Unknown
Glutamate
Sucrose
Contribution Corr(tp, X)
Covariance Cov(tp, X)
R2X[1] = 0.322
c
Camalexin
**
Mock AgN23
I3M
**
Mock AgN23
Peak Area (A.U.)
d
Scores Plot
Col-0
Col-0 + AgN23
pad3
pad3 + AgN23
QC
PC 2 (11.3 %)
PC 1 (66.2 %)
e
Camalexin
****
Mock
AgN23
Peak Area (A.U.)
col-0
pad3

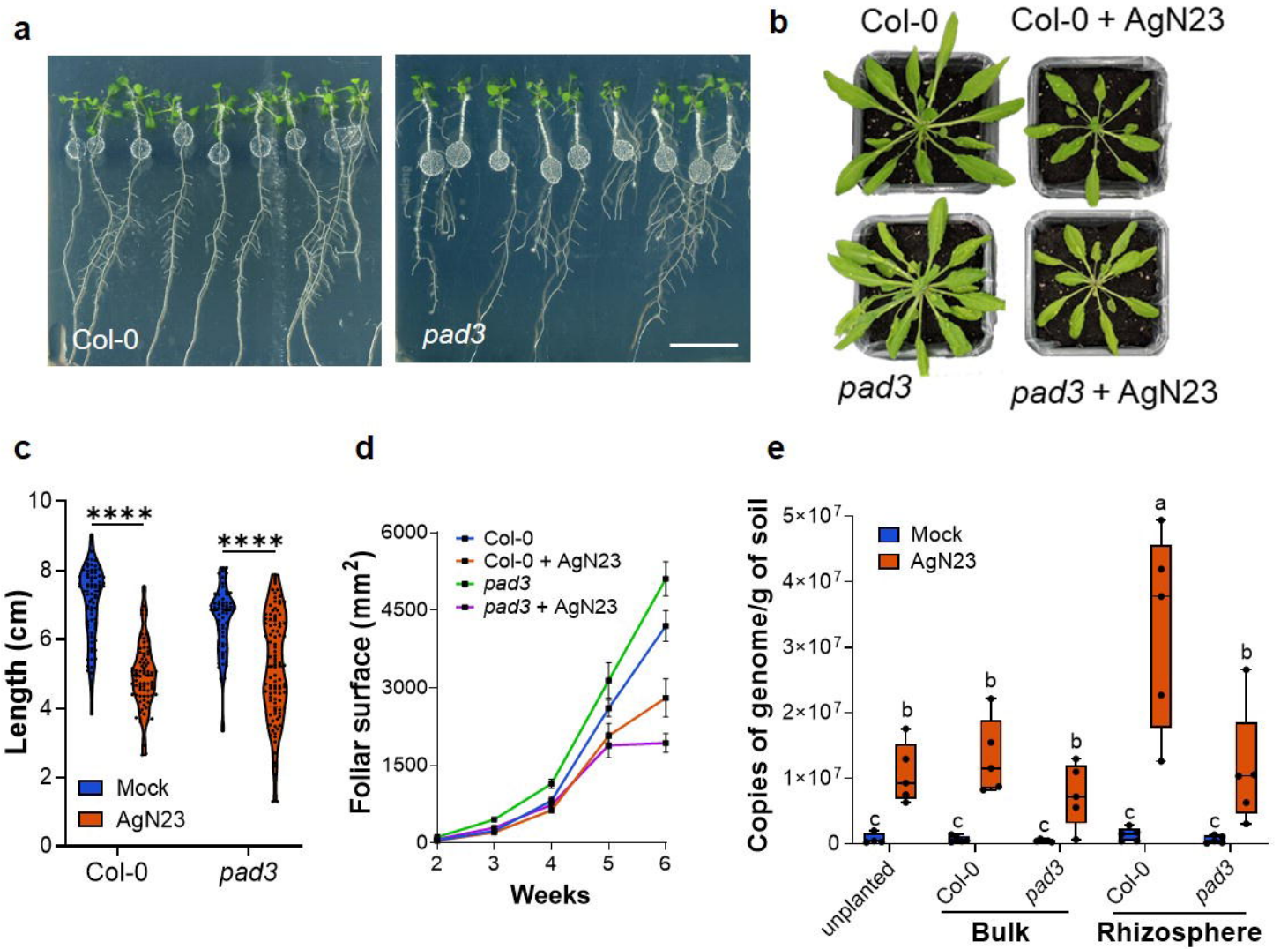
a
Col-0
pad3
b
Col-0
Col-0 + AgN23
pad3
pad3 + AgN23
c
****
****
Length (cm)
Mock
AgN23
Col-0
pad3
d
Foliar surface (mm²)
Col-0
Col-0 + AgN23
pad3
pad3 + AgN23
Weeks
e
Copies of genome/g of soil
Mock
AgN23
unplanted
Col-0
pad3
Col-0
pad3
Bulk
Rhizosphere

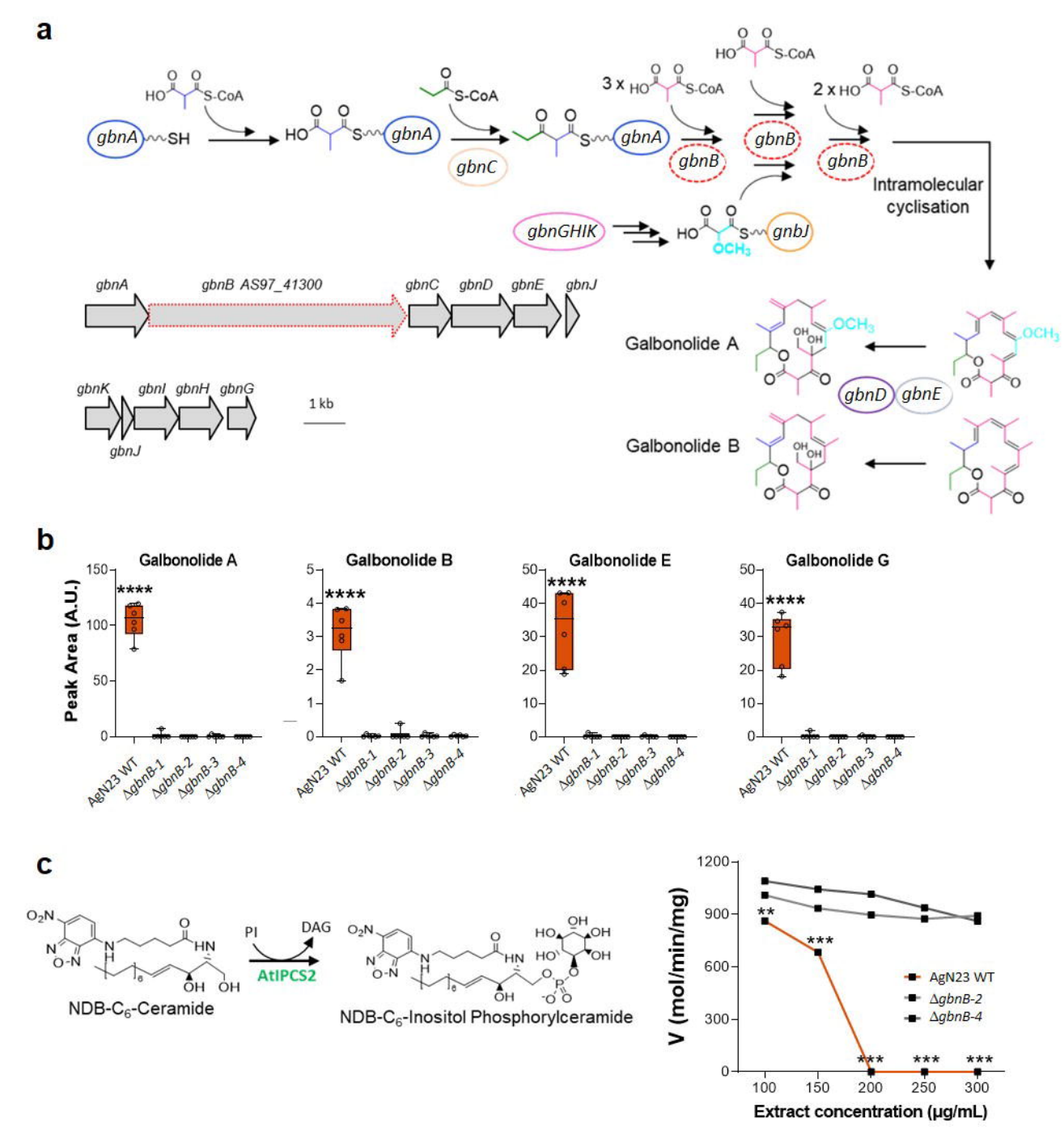
a
gbnA
SH
S-CoA
HO
gbnC
3 x
2 x
gbnB
gbnGHIK
gnbJ
OCH3
Intramolecular cyclisation
gbnA
gbnB AS97_41300
gbnC
gbnD
gbnE
gbnJ
gbnK
gbnI
gbnH
gbnG
1 kb
Galbonolide A
Galbonolide B
gbnD
gbnE
b
Galbonolide A
Galbonolide B
Galbonolide E
Galbonolide G
Peak Area (A.U.)
****
AgN23 WT
ΔgbnB-1
ΔgbnB-2
ΔgbnB-3
ΔgbnB-4
c
NDB-C6-Ceramide
PI
DAG
AtIPCS2
NDB-C6-Inositol Phosphorylceramide
V (mol/min/mg)
Extract concentration (µg/mL)
AgN23 WT
ΔgbnB-2
ΔgbnB-4
**
***

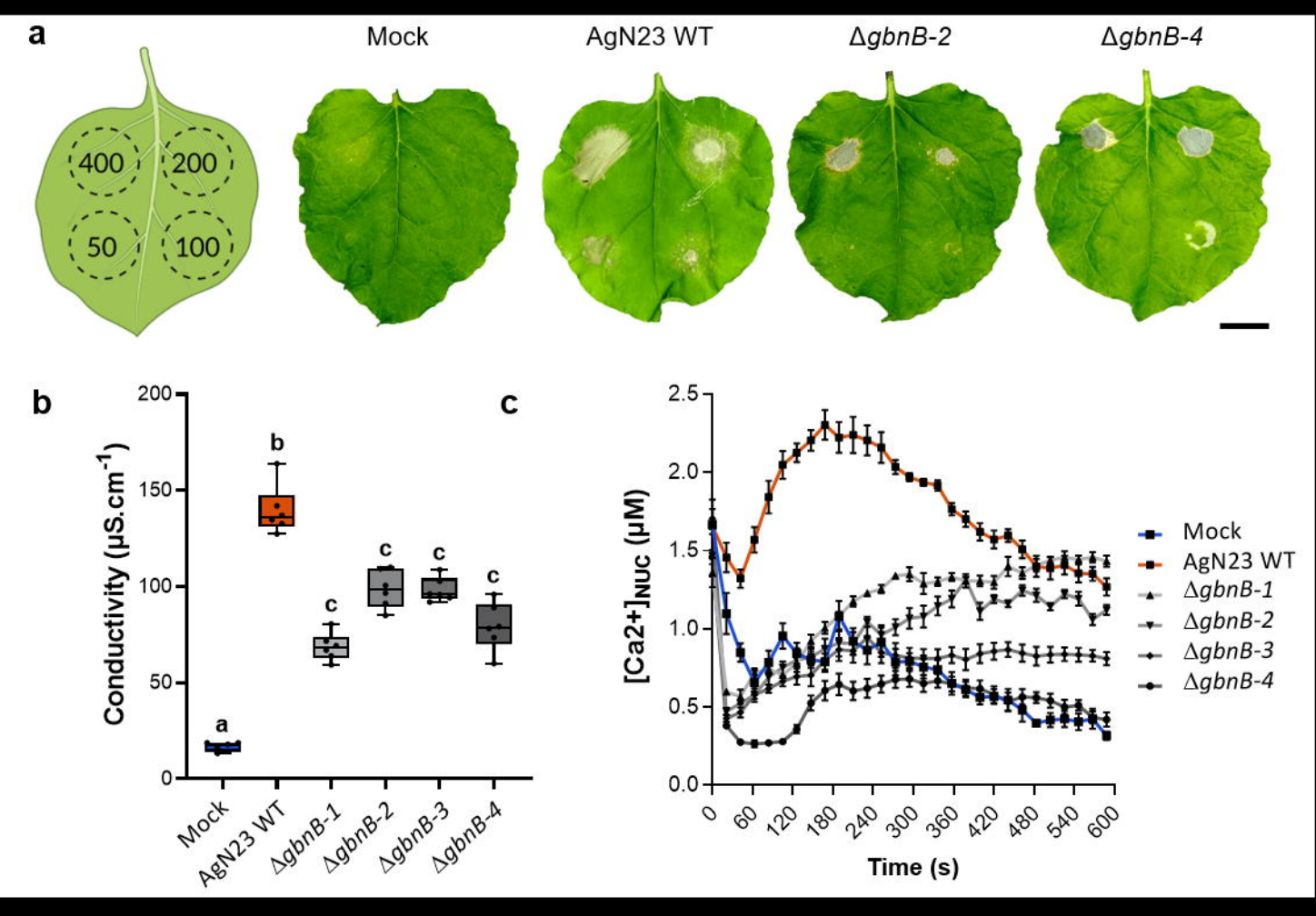
a
Mock
AgN23 WT
ΔgbnB-2
ΔgbnB-4
400
200
50
100
b
Conductivity (µS.cm-1)
200
150
100
50
0
a
b
c
c
c
c
Mock
AgN23 WT
ΔgbnB-1
ΔgbnB-2
ΔgbnB-3
ΔgbnB-4
c
[Ca2+]NUC (µM)
2.5
2.0
1.5
1.0
0.5
0.0
0
60
120
180
240
300
360
420
480
540
600
Time (s)
Mock
AgN23 WT
ΔgbnB-1
ΔgbnB-2
ΔgbnB-3
ΔgbnB-4

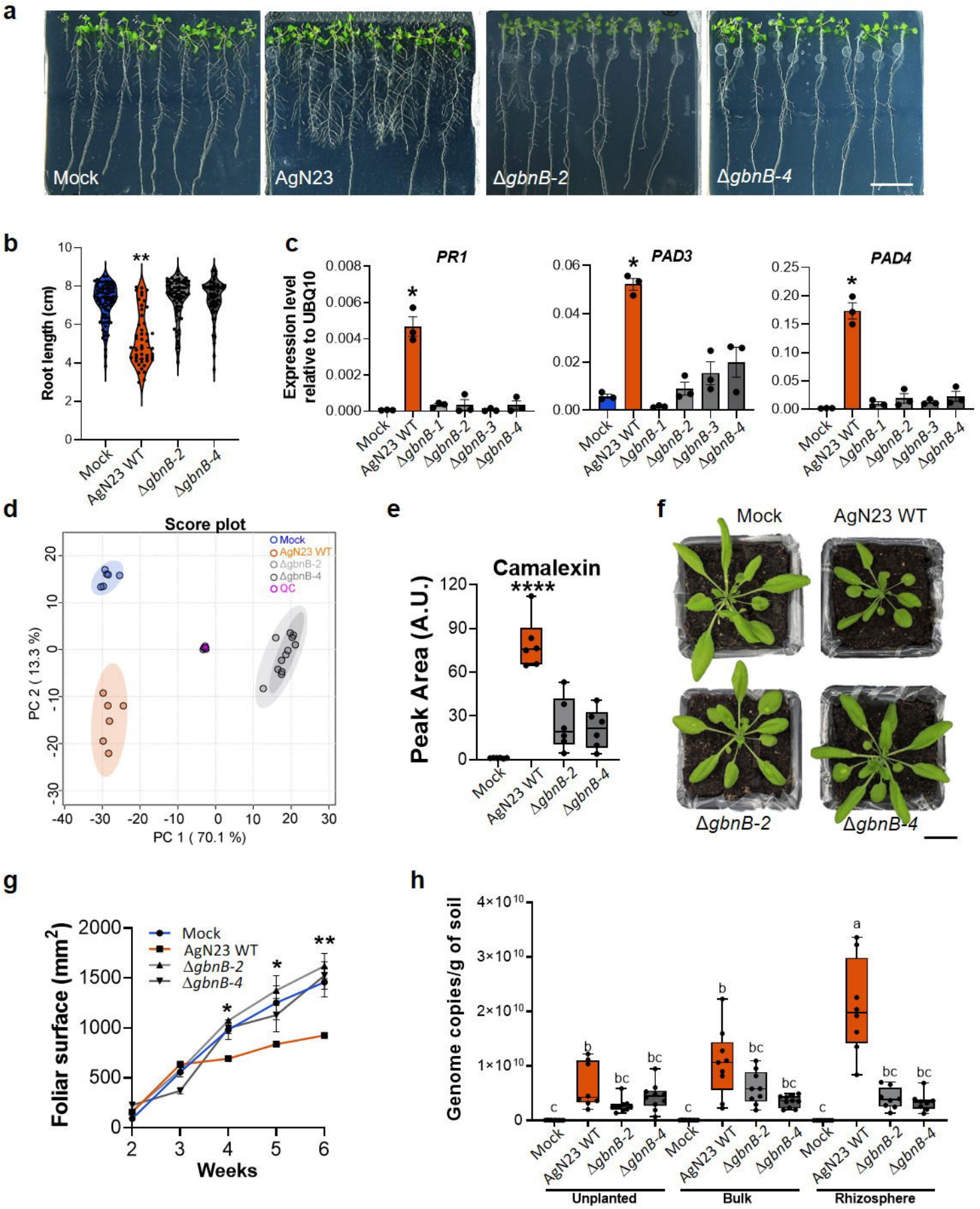
a
Mock
AgN23
ΔgbnB-2
ΔgbnB-4
b
Root length (cm)
Mock
AgN23 WT
ΔgbnB-2
ΔgbnB-4
c
Expression level relative to UBQ10
PR1
PAD3
PAD4
Mock
AgN23 WT
ΔgbnB-1
ΔgbnB-2
ΔgbnB-3
ΔgbnB-4
d
Score plot
Mock
AgN23 WT
ΔgbnB-2
ΔgbnB-4
QC
PC 1 (70.1 %)
PC 2 (13.3 %)
e
Camalexin
Peak Area (A.U.)
Mock
AgN23 WT
ΔgbnB-2
ΔgbnB-4
f
Mock
AgN23 WT
ΔgbnB-2
ΔgbnB-4
g
Foliar surface (mm²)
Mock
AgN23 WT
ΔgbnB-2
ΔgbnB-4
Weeks
h
Genome copies/g of soil
Mock
AgN23 WT
ΔgbnB-2
ΔgbnB-4
Unplanted
Bulk
Rhizosphere

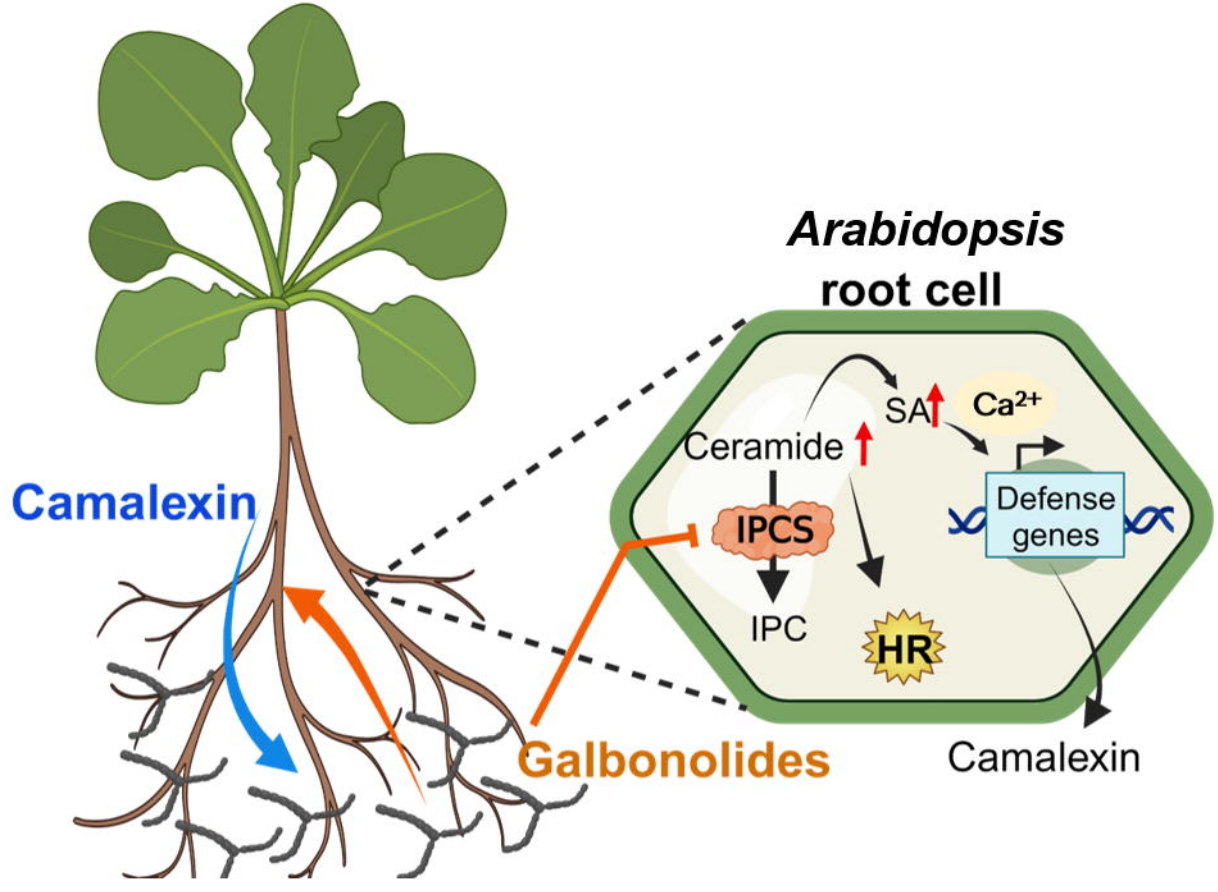

Streptomyces* sp. *AgN23